J. Phys.: Condens. Matter **9** (1997) 8945–8961. Printed in the UK PII: S0953-8984(97)85005-9

Effect of deformation on low-temperature deuteride precipitation in single crystal niobium

Brent J Heuser† and John W Althauser‡

† University of Illinois, Department of Nuclear Engineering, Urbana, IL 61801, USA
‡ University of Illinois, Department of Materials Science, Urbana, IL 61801, USA

Received 9 June 1997

Abstract. Small-angle neutron scattering (SANS) measurements of low concentration, single crystal Nb–D alloys have been performed to characterize the effect of deformation on deuteride phase formation. The SANS response from the deuteride phase formed at low temperature in the undeformed matrix was consistent with a spherical particle morphology, as expected from a large body of published TEM studies. In addition, a significant hysteresis was observed ($\Delta T \sim 100^{\circ}$) in the SANS response versus temperature from the undeformed sample material. The hysteresis is attributed to the irreversible plastic deformation required to nucleate the incoherent phase. Deformation produced by unidirectional rolling to 50% thickness reduction altered the deuteride phase transformation characteristics in a fundamental way. The SANS response was highly anisotropic, indicative of an oriented, anisometric particle morphology. Metallographic analysis of deformed specimens electropolished below the solvus temperature confirmed the presence of large deuteride plates with an orientation consistent with the anisotropic SANS response. Deformation also eliminated the temperature hysteresis observed in the undeformed material. A cellular dislocation substructure was found in TEM characterization of the deformed Nb single crystal material. The plate-like particle morphology in the deformed material is attributed to an interaction between the precipitating deuterium and the cellular dislocation substructure. The elimination of the temperature hysteresis is consistent with an interaction between the deuterium and regions of high dislocation density facilitating heterogeneous nucleation.

1. Introduction

Phase transformations in the Nb–H system have been of interest for quite some time. Theoretical calculations have been performed for the α–α' portion of the phase diagram using a lattice gas model modified to include hard-core repulsion and elastic interactions between protons [1, 2]. These efforts were found to be in reasonable agreement with the known phase diagram [2]. On the experimental side, coherent and incoherent hydrogen precipitation in Nb has been observed by *in situ* x-ray diffraction [3, 4]. One especially interesting aspect of this work was the observation of sample-shape-dependent hydrogen concentration modes within the coherent portion of the α–α' phase diagram [4], consistent with earlier theoretical work [2, 5].

Numerous transmission electron microscopy studies of *in situ* precipitation [6–9] have led to a general consensus of the incoherent phase diagram and associated phase structures [10]. Of relevance here is the observation of small, spherical or cube-shaped particles in the low temperature, low concentration portion (ε phase) of the Nb–H phase diagram [6]. In fact, the conditions investigated by Schober in [6] (hydrogen concentrations less than 5%, temperatures of approximately 110 K) are similar to those studied here.

0953-8984/97/428945+17$19.50

Although TEM, electron and x-ray diffraction are invaluable in the determination of hydride phase structures and morphologies, these techniques suffer from low sensitivity to hydrogen in metal lattices. It is important to note, though, that this limitation does not prevent the observation of superlattice reflections from ordered hydride phases [8]. However, in the absence of an ordered hydrogen superlattice, electron and x-ray based techniques derive all structural and morphological information from changes in the host lattice brought on by the incorporation of hydrogen.

Neutron-based techniques such as neutron diffraction and small-angle neutron scattering (SANS) have a much greater sensitivity to the presence of deuterium (hydrogen). (Generally, deuterium is used in coherent neutron scattering measurements. The coherent scattering cross section of the deuteron is three times larger than that of the proton, while the incoherent scattering cross section is a factor of 40 lower.) Neutron diffraction measurements of the Nb–D system have been performed, but have been limited to high concentration alloys [9, 10]. Perhaps this is due to the fact that even in neutron diffraction measurements, a limit of a few volume percent exists for the resolution and refinement of second phase structures.

In contrast, SANS is extremely sensitive to deuterium precipitation in a metal lattice. Deuteride particle shape and local deuterium concentration can be determined from analysis of SANS data using simple models. The ability to examine *in situ* deuterium precipitation low-concentration alloys on a bulk scale can provide information that is otherwise difficult to obtain.

2. Experimental details

Single crystal Nb samples were taken from a 99.9% pure Nb single crystal ingot with a [110] cylinder axis. This ingot was prepared using a zone refining technique by Metal Crystals and Oxides Ltd of Cambridge, England. Samples were cut from this ingot with faces normal to the cylinder axis direction. Deuterium loading was performed *ex situ* by exposure to D_2 gas at 673 K after a one hour, 10^{-7} Torr, vacuum anneal at 1073 K. This operation was performed in an all metal vacuum manifold with a quartz sample tube. Deuterium concentrations were determined by the volumetric technique and from the change in mass. Concentrations of a given sample determined by these two methods typically agreed to within 10%. The deuterium concentrations for all samples presented here were such that only the solid solution, α phase existed at room temperature. Hydrogen and deuterium absorption into and evolution from Nb at room temperature up to approximately 500 K does not occur. (This effect is usually attributed to the native oxide acting as a permeation barrier and/or as surface that limits dissociation and recombination. However, evidence of an alternative mechanism involving a sub-surface trapping interaction has been proposed [11].) The loaded samples could therefore be handled, stored, transported and measured without any special precautions to limit deuterium outgassing.

SANS measurements of five single crystal samples are presented here; a low concentration set (identified by 'lc') of three samples with 7000 to 8000 atomic parts per million (appm) deuterium and a higher concentration set (identified by 'hc') of two samples with 24000–25000 appm deuterium. One sample from each set was deformed to 50% thickness reduction by unidirectional rolling at room temperature (identified by 'd') after deuterium loading. Rolling was performed using 5 inch diameter slow-speed steel rollers. Eight to ten passes were required to achieve the final thickness reduction. The rolling direction was $[1\bar{1}1]$ and the direction of thickness reduction corresponded to the [110] face-normal axis.

SANS measurements were performed at the Intense Pulsed Neutron Source (IPNS) at the Argonne National Laboratory in Argonne, Illinois using the Small-Angle Diffractometer (SAD) instrument [12]. IPNS is a spallation neutron source with time-of-flight (TOF) based scattering instruments. For the SANS technique, two dimensional scattering patterns are recorded as a function of TOF (or neutron wavelength) and folded together during automated data reduction. Multiple Bragg diffraction from crystalline samples is possible for neutron wavelengths shorter than the Bragg cut-off. The problem is especially severe for single crystals, but is easily avoided by rejecting all data in TOF bins below the cut-off. In principle, a Q range of $0.006 \leqslant Q \leqslant 0.1$ Å^{-1} (the wave-vector transfer, Q, is given by $Q = (4\pi/\lambda)\sin\theta$, where λ is the neutron wavelength and θ is half the scattering angle) can be probed for crystalline samples with the SAD, although the actual range may be reduced for weakly scattering systems. SANS measurements were corrected for sample transmission, empty beam, and dark current. Absolute macroscopic differential scattering cross sections were determined by using a polymer standard sample [12].

All SANS measurements were performed in vacuum using a Displex capable of 12 K operation. Except for the sample, two beam defining Cd apertures (before and after the sample), and the two sapphire vacuum-jacket windows, no other material was placed in the neutron beam. Sample temperature during SANS investigation was monitored with a thermocouple mounted near the sample on the sample holder. This sample holder was fabricated from 1100F aluminium and mounted directly to the Displex cold finger.

Maximum cooling rates of 2–3 °C min^{-1} at the sample location were typically observed. The thermocouple calibration, checked at 77 K and 273 K, was found to read 1–2 degrees too low. This was considered adequate and all temperatures reported here are not corrected for this slight inaccuracy.

3. Results and discussion

3.1. Effect of crossing the low-temperature solvus

The 293 and 120 K SANS response from Nb1(lc), an undeformed, single crystal Nb sample loaded with 7400 appm deuterium, is shown in figure 1. (All data are presented as radial averages over all azimuthal angles recorded by the 2D SANS detector unless otherwise stated.) The incoherent solvus (in this case, $\alpha \rightarrow \varepsilon$ solvus) at 7400 appm is approximately 210 K. (Although some uncertainty in the Nb–H phase map exists [10], the low temperature, low concentration phase is referred to as 'ε' here.) Thus, the effect of crossing the solvus on the observable scattering response is illustrated by this measurement. The scattering response at 120 K represents a 50- to 60-fold increase over the 293 K measurement at lowest Q. Based on an application of the lever rule at 120 K, approximately 1–2% of the total volume of the Nb matrix was converted to the ε phase.

The SANS response of two low concentration samples, Nb1(lc) and Nb9(lc/d), at 120 K are compared in figure 2. This figure is in ln–ln format, allowing the identification of power law scattering behaviours ($\mathrm{d}\Sigma/\mathrm{d}\Omega \sim 1/Q^n$). Nb9(lc/d) was prepared with 7800 appm deuterium and was deformed by unidirectional rolling to 50.7% thickness reduction. As with Nb1(lc), this sample was cooled continuously from room temperature to 120 K at the maximum cooling rate. The deformation of Nb9(lc/d) has a noticeable effect on the observed SANS response. In particular, the high-Q power law behaviour is changed from $\mathrm{d}\Sigma/\mathrm{d}\Omega \propto Q^{-4}$ (Nb1(lc)) to $\mathrm{d}\Sigma/\mathrm{d}\Omega \propto Q^{-2}$ (Nb9(lc/d)). Q^{-4} behaviour is still present in the Nb9(lc/d) measurement, but is much weaker and occurs at the low-Q end of the measured range.

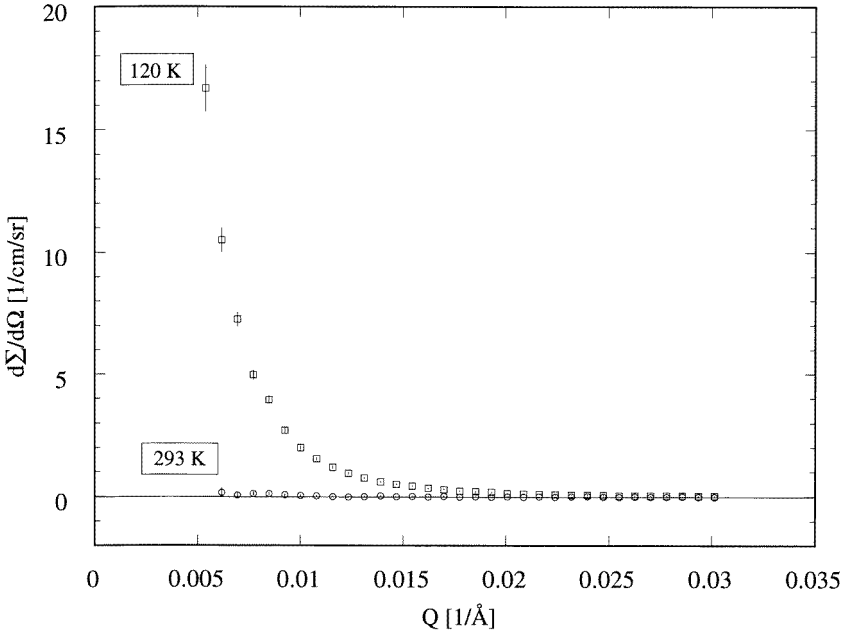

Figure 1. 293 K (open circles) and 120 K SANS (open squares) response of Nb1(lc), a lower concentration undeformed single crystal Nb sample.

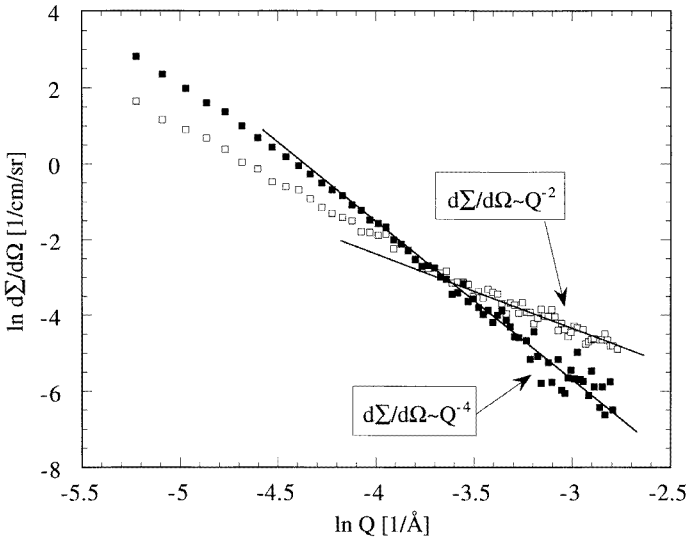

Figure 2. 120 K SANS measurement of lower concentration samples, undeformed Nb1(lc) (full squares) and deformed Nb9(lc/d) (open squares). Deformation resulted in a pronounced Q^{-2} response at the high-Q end of the measurement.

The 120 K measurement of the two high concentration samples, Nb6(hc) and Nb8(hc/d), are compared in figure 3. Nb6(hc) was undeformed and had a deuterium concentration of 24 000 appm. Nb8(hc/d) was loaded to 24 500 appm deuterium and deformed by

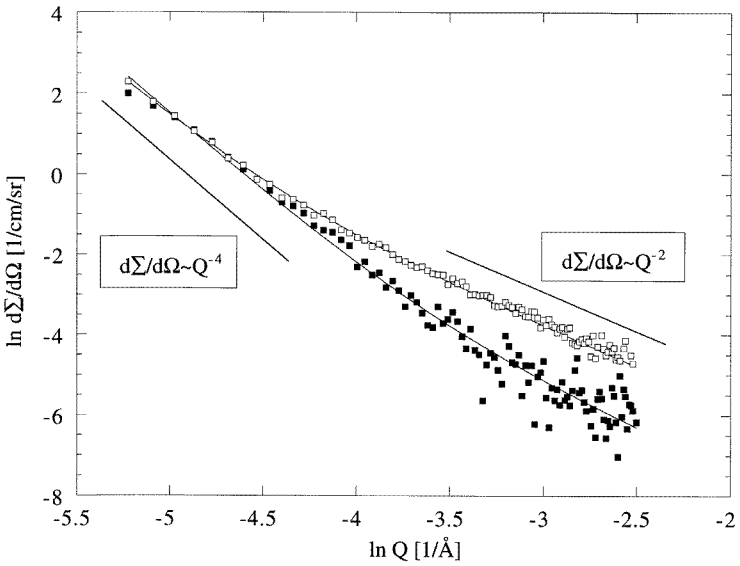

Figure 3. 120 K SANS measurement of higher concentration samples, undeformed Nb6(hc) (full squares) and deformed Nb8(hc/d) (open squares). Solid lines are best fits of a $d\Sigma/d\Omega \propto Q^{-2} + Q^{-4}$ behaviour. Amplitudes of the Q^{-2} and Q^{-4} responses are given in table 1.

unidirectional rolling to 49.5% thickness reduction. Unlike the previous samples, both Nb6(hc) and Nb8(hc/d) were step-wise cooled, with SANS patterns recorded at constant temperature every 40–50 degrees. This was done to observe the effect of deformation on the phase transformation temperature hysteresis and is discussed below. Like Nb9(lc/d), a significant Q^{-2} response is observed at high-Q end of the Nb8(hc/d) measurement. Sample characteristics and SANS results, given by radially averaged Q^{-2} and Q^{-4} amplitudes, are compiled in table 1. The results from Nb7(lc), an undeformed, low concentration sample that was stepwise cooled, are also included in this table.

The Q^{-4} response, known as Porod behaviour, results from discontinuous changes in the nuclear scattering length density. Such discontinuities may occur at the internal surfaces or interfaces, such as those associated with voids and second phase particles, for example. The Porod response is an asymptotic behaviour valid for all Q such that $Q\mathcal{D} \gg 1$, where $\mathcal{D}$ is the characteristic dimension of the scattering object, and is given by [13],

$$\frac{d\Sigma}{d\Omega}(Q) = \frac{4\pi\,\Delta\rho^2}{Q^4}\frac{S}{V} \tag{1}$$

where $\Delta\rho$ is the scattering length density contrast, in the present case between the ε deuteride phase and the Nb solid solution α phase ($\Delta\rho \cong 2.9 \times 10^{10}$ cm^{-2}), S is the total interfacial surface area, and V is the irradiated sample volume. This equation represents an average over all scattering object orientations and therefore does not directly provide morphological information. However, for oriented, highly anisometric particles, the Porod response can exhibit severe anisotropy.

Equation (1) can be used to calculate the total deuteride surface per unit volume for the undeformed samples. The results of this calculation for the 120 K data are shown in table 2. The total volume fraction of the deuteride phase at 120 K (from the application of the lever rule to the equilibrium Nb–H phase diagram) is also given in table 2. Equation (1)

Table 1. Power-law amplitudes for 120 K SANS measurements of Nb–D samples.

Sample	$D_{conc.}$ [appm]	Deformation	Q^{-4} amplitude ($\times 10^{-9}$ cm^{-1} Å^{-4} sr^{-1})	Q^{-2} amplitude ($\times 10^{-5}$ cm^{-1} Å^{-2} sr^{-1})
Nb1(lc)*	7400	undeformed	22.6 ± 1.0	—
Nb9(lc/d)*	7800	50.7% (unidirectional)	5.0 ± 0.3	2.9 ± 0.1
Nb7(lc)	7000	undeformed	2.8 ± 0.4	0.7 ± 0.1
Nb6(hc)	24000	undeformed	9.0 ± 0.1	1.1 ± 0.1
Nb8(hc/d)	24500	49.5% (unidirectional)	6.6 ± 0.4	5.5 ± 0.1

* Cooled continuously from 293 K to 120 K at 2–3 °C min^{-1}. All others step-wise cooled.

Table 2. Low temperature deuteride phase parameters determined from SANS.

Sample	Volume fraction of ε phase from lever rule	S/V (cm^{-1})	f, volume fraction of ε phase giving Q^{-2} response
Nb1(lc)*	0.02	214	—
Nb9(lc/d)*	0.02	—	0.0025
Nb7(lc)	0.02	26.5	—
Nb6(hc)	0.06	85.2	—
Nb8(hc/d)	0.06	—	0.0050

* Cooled continuously from 293 K to 120 K at 2–3 °C min^{-1}. All others step-wise cooled.

is not applied to the deformed sample data. As demonstrated below, deformation resulted in the formation of oriented, plate-like deuteride particles. The general form of the Porod law given by equation (1) represents an average over all particle orientations [13]. This condition is automatically satisfied for a spherical particle shape. It is not, however, met for oriented anisometric particles, even when the radial average cross section is used.

Notice from table 1 that the Porod response of the Nb1(lc) is 2.5 times greater than that of Nb6(hc) and 8.1 times greater than that of Nb7(lc). This appears to be inconsistent with the known deuterium loading. Also recall that the Porod response of Nb1(lc) occurred at the high-Q end of the measured range (figure 2), whereas it occurs at the low-Q end for all other samples. This latter point is demonstrated for Nb6(hc) in figure 4; a pure, low-Q Porod behaviour results after subtraction of the small Q^{-2} component. These observations are consistent with smaller, more finely dispersed deuteride particles in Nb1(lc) and is attributed to the cooling rate; continuous for Nb1(lc) versus step-wise for Nb6(hc) and Nb7(lc). This hypothesis is corroborated most strongly by the results of Nb7(lc). This sample was undeformed, loaded to 7000 appm deuterium, and step-wise cooled; in other words, identical to Nb1(lc) except for the cooling rate. The effect of cooling rate on observed SANS response is dramatic; a factor of 8.1 increase in Porod amplitude.

The other relevant comparison of Porod amplitudes is between Nb6(hc) and Nb7(lc), both of which underwent approximately the same step-wise cooling procedure. Here the scattering amplitudes are almost in direct proportion of the deuterium concentration. This is expected if the relative number of deuteride particles versus particle size (the normalized size distribution) are equal for the two samples. In this case, the total deuteride surface area will scale with the total amount of deuterium available for phase transformation.

A single crystal Nb reference sample, deformed to 50% thickness reduction by rolling at room temperature and without deuterium loading, was measured at 293 K and 175 K

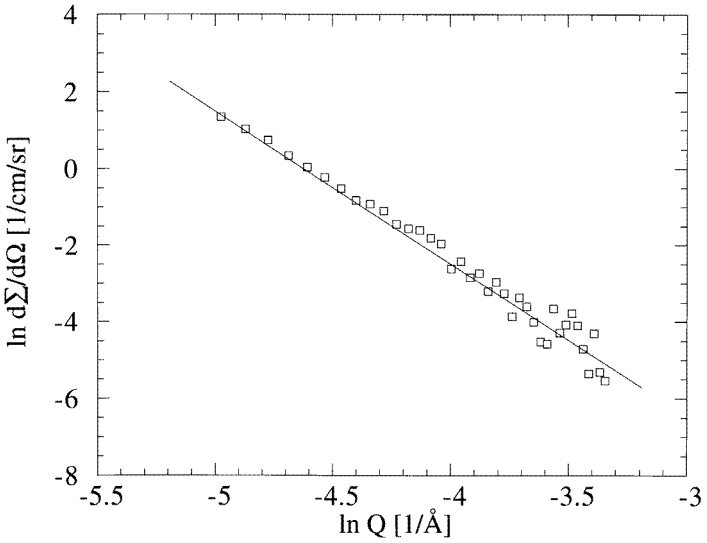

Figure 4. Residual Q^{-4} SANS response of Nb6(hc) after subtraction of Q^{-2} response.

(measurement not shown). The purpose of this measurement was to confirm that the large increases in SANS response reported here were due to deuterium precipitation in the deuterium-loaded samples. As expected, the scattering response of the reference sample was low and remained invariant with respect to temperature.

3.2. Scattering anisotropy

The most striking effect of deformation was the development of significant anisotropy in the scattering pattern. Responses from all three undeformed samples, Nb1(lc), Nb6(hc), and Nb7(lc), were isotropic, consistent with a spherical deuteride particle morphology. Although randomly oriented particles of any shape would exhibit any isotropic scattering pattern, spherical hydride particles have been observed under similar conditions (113 K, hydrogen concentrations less than 5%) with *in situ* TEM by Schober [6]. On the other hand, the scattering patterns of both Nb8(hc/d) and Nb9(lc/d) exhibited a pronounced two-fold symmetry in the region of Porod scattering below $Q < 0.03$ Å^{-1}. This anisotropy is quantified in figures 5 and 6, which show the dependence of Porod and Q^{-2} scattering amplitudes as a function of detector azimuthal angle, θ, for Nb8(hc/d) and Nb9(lc/d), respectively. Both samples were oriented with the $[1\bar{1}1]$ rolling direction at $\theta = 0^\circ$ and have the same, strongly peaked anisotropy. This can only occur for oriented, highly anisometric particles. The radially averaged Porod and Q^{-2} amplitudes given in table 1 can now be identified as averages over all azimuthal angles ($-\pi/2 \leqslant \theta \leqslant \pi/2$) in figures 5 and 6.

The severe anisotropy of the Porod response is attributed to an oriented arrangement of large plate-like particles. Scattering from plate-like particles is expected to be highly peaked about an axis perpendicular to the face normal of the plate. This is a direct consequence of the inverse relationship between particle dimension and scattering angle or Q. The small-angle scattering response is compressed into a small angular or Q range about $Q = 0$ along in-plane directions of the plate. The resultant scattering then becomes highly peaked about

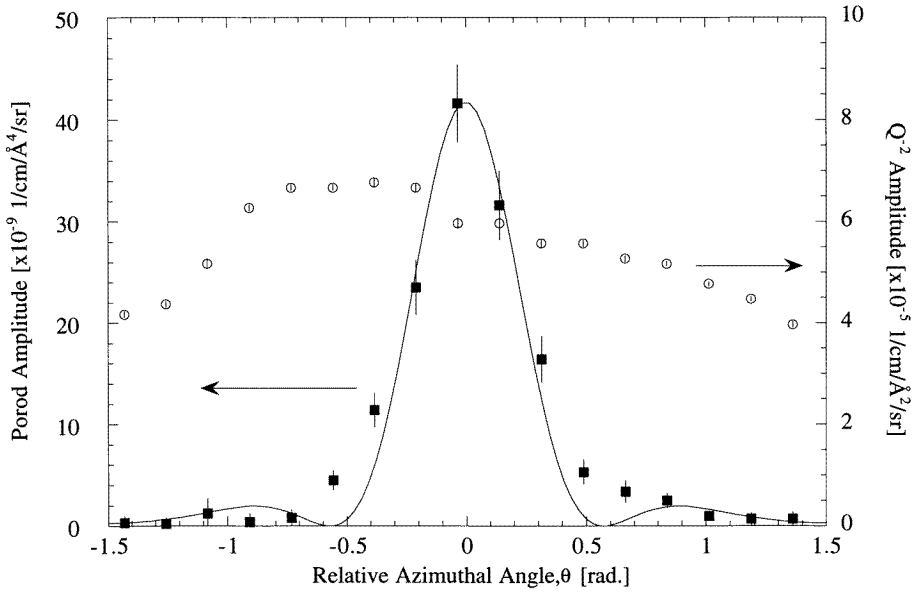

Figure 5. Porod and Q^{-2} amplitudes as a function of detector azimuthal angle, θ, for deformed, high deuterium concentration sample Nb8(hc/d). The solid curve is a best fit of equation (2) to the observed Porod amplitude dependence on θ. Only half of the total 2π azimuthal angles are shown because of the two-fold symmetry of the SANS response. The $[1\bar{1}1]$ rolling direction corresponds to $\theta = 0$.

the plate normal direction. The fall-off in intensity from the face normal direction is given qualitatively by [14],

$$\frac{d\Sigma}{d\Omega}(Q) \sim [\sin(\pi\alpha)/\pi\alpha]^2 \tag{2}$$

where α is the product of the plate dimension and Q component in the plane of the plate (the latter of which is proportional to $\sin\theta$). The anisotropic responses of the deformed samples shown in figures 5 and 6 follow this general behaviour reasonably well.

3.3. $1/Q^2$ *behaviour*

The most noticeable effect of deformation in figures 2 and 3 is the development of Q^{-2} scattering at higher Q. Unlike the low-Q Porod scattering from the deformed samples, this scattering is isotropic (see figures 5 and 6). A Q^{-2} response is the single particle form factor of an object with plate-like geometry. The macroscopic differential scattering cross section is given by the product of the single particle form factor and the plate number density [15],

$$\frac{d\Sigma}{d\Omega}(Q) = 2\pi N_P A T^2 \frac{\Delta\rho^2}{Q^2} \exp(-Q^2T^2/12) \cong 2\pi f T \frac{\Delta\rho^2}{Q^2} \tag{3}$$

where N_P is the number density of deuteride plate-like particles, A is the plate cross-sectional area, T is the plate thickness, f is the volume fraction of particles resulting in the Q^{-2} response and $\Delta\rho$ is the scattering length density contrast as given above. The right-hand side of equation (3) is written under the assumption that $QT \leqslant 1$. This is justified because a pure Q^{-2} response was observed in the high-Q limit of the measurement.

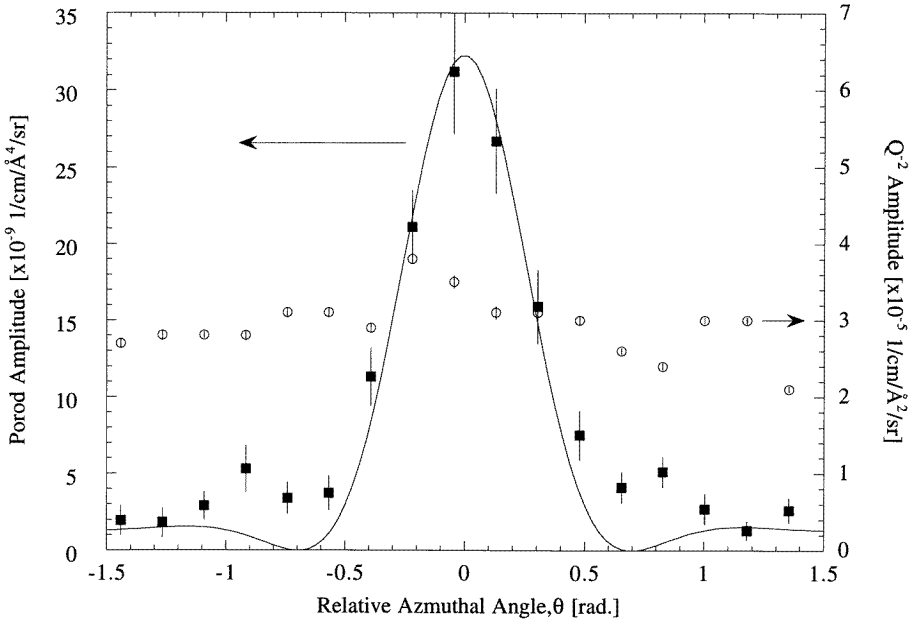

Figure 6. Porod and Q^{-2} amplitudes as a function of detector azimuthal angle, θ, for deformed, LOW deuterium concentration sample Nb9(lc/d). The solid curve is a best fit of equation (2) to the observed Porod amplitude dependence on θ. Only half of the total 2π azimuthal angles are shown because of the two-fold symmetry of the SANS response. The $[1\bar{1}1]$ rolling direction corresponds to $\theta = 0$.

It is important to distinguish between the two types of plate-like particles resulting in the Porod and Q^{-2} scattering responses observed from the deformed samples, because they are different. Porod scattering is an asymptotic behaviour that occurs beyond the Q range where the single particle form factor dominates. Thus, the Porod scattering observed from the deformed samples cannot be the asymptotic response of the plate-like particles causing the Q^{-2} behaviour because it occurs at lower, not higher, Q. The 'Porod' deuteride particles would also exhibit a Q^{-2} form factor, but at much lower Q than probed in these measurements. Likewise, the 'Q^{-2}' particles would exhibit a Porod response in a range beyond the maximum Q measured here. That the Q^{-4} scattering is highly anisotropic, while the Q^{-2} response is isotropic, is another indication that two distinct sets of deuteride precipitate plates are present.

The observation of the Q^{-4} behaviour at low-Q implies that the thickness of the 'Porod' plates must be very large, so that $QT \gg 1$ is satisfied at the *lowest* Q limit of the measurement. An estimate of the *minimum* thickness can be made; $T \geqslant 2000$ Å ($T \gg 1/0.005$ Å). On the other hand, the 'Q^{-2}' plates must satisfy $QT \leqslant 1$ at the highest Q of the measurement, leading to an estimated *maximum* thickness of approximately 20 Å.

The volume fraction of deuteride particles responsible for the Q^{-2} scattering observed from Nb8(hc/d) and Nb9(lc/d) can be estimated using equation (3) if the plate thickness is known. Setting $T = 20$ Å in equation (2) leads to volume fractions of 0.0050 and 0.0025 for Nb8(hc/d) and Nb9(lc/d), respectively. This simple analysis demonstrates that the total volume fraction of the 'Q^{-2}' plates is very small, much smaller than the total ε

phase volume fraction estimated from the phase diagram (see table 2). The balance of the precipitated deuterium is in the much larger 'Porod' plates.

We note that the initial trapping of deuterium at dislocations can result in a SANS response. The deuterium-dislocation trapping interaction, in the absence of deuteride formation, has been investigated with SANS in single crystal Pd [16, 17]. The response from this trapping interaction is very weak ($d\Sigma/d\Omega \sim 0.02 - 0.03$ cm^{-1} sr^{-1} at $Q \sim 0.01$ Å^{-1}) and would be dominated by the large deuteride SANS response observed below the solvus temperature. In principle, the SANS response from the trapping interaction could be seen at temperatures above the solvus. This would require impractical counting times on the SAD instrument and was not attempted in this study.

3.4. Temperature hysteresis

The SANS response during step-wise cooling, followed by step-wise heating, of Nb7(lc) is shown in figure 7. Equilibrium at each temperature was confirmed by an invariant scattering response. However, this procedure was not sensitive to slowly varying changes. The ordinate in figure 7 is the absolute scattering cross section integrated over the entire Q range. A substantial hysteresis about the incoherent $\alpha \rightarrow \varepsilon$ solvus is evident.

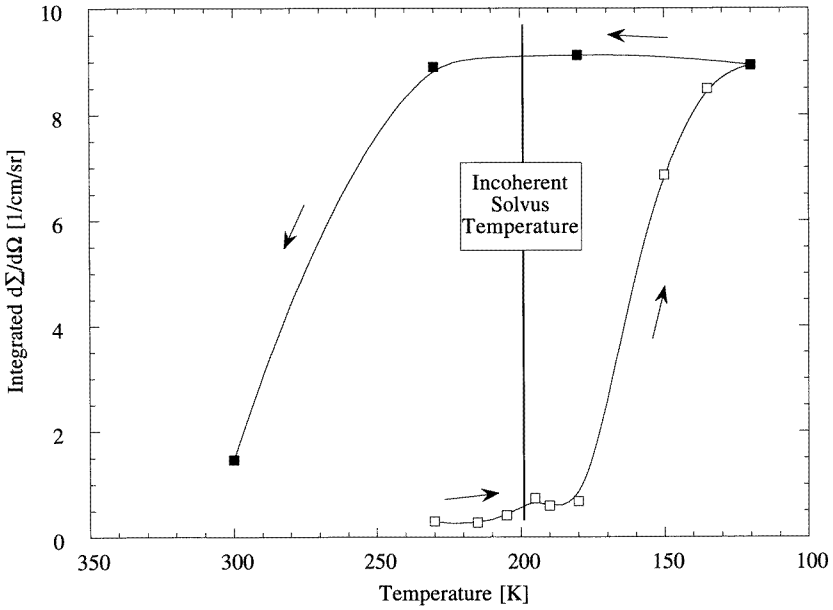

Figure 7. Integrated $d\Sigma/d\Omega$ for Nb7(lc) as a function of sample temperature during *in situ* step-wise cooling and heating. Arrows indicate direction of temperature change. The integrated scattering response shows a significant hysteresis associated with nucleation and reversion of the deuteride phase.

The temperature-dependent scattering amplitudes of the Q^{-4} and Q^{-2} behaviours for Nb8(hc/d) are shown in figures 8 and 9, respectively. The Porod amplitude in figure 8 was determined along the direction of most intense scattering ($\theta = 0$ in figure 5), while the Q^{-2} amplitude in figure 9 is a radial average. Although fewer temperature steps were measured for this sample, a few observations can be made. First, the Porod

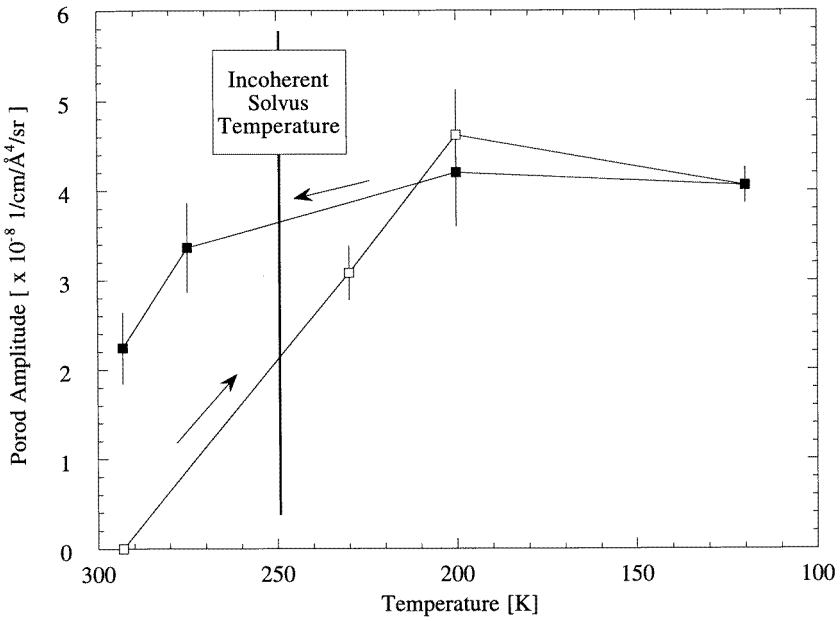

Figure 8. Porod amplitude for Nb8(hc/d) as a function of sample temperature during *in situ* step-wise cooling and heating. Arrows indicate direction of temperature change. The Porod response increases immediately upon crossing the incoherent solvus temperature.

response changes immediately upon crossing the solvus temperature during both cooling and heating. Likewise, the Q^{-2}, plate-like responses track closely together in figure 9, although apparently this behaviour is responding to a lower incoherent solvus temperature. This latter observation is consistent with a smaller amount of solid-solution deuterium available for Q^{-2} platelet formation; the incoherent solvus temperature corresponding to 2500 appm deuterium (one tenth of the total deuterium concentration in accordance with f in table 2) is approximately 175 K [10].

Temperature hystereses similar to that in figure 7 have been observed in resistivity measurements performed by Westlake and Ockers [18] and by Birnbaum *et al* [19] on low concentration Nb–H (–D) alloys. Hystereses in systems with large phase transformation volume differences are generally thought to be due to irreversible plastic deformation during incoherent hydride formation [18]. This hypothesis has been corroborated by the observed dependence of solvus temperature on temperature cycle history; thermal cycling through the two phase region was found to reduce the hysteresis, consistent with heterogeneous nucleation at remnant dislocations from previous cycles [19]. The behaviour of Nb8(hc/d) in figures 8 and 9 is consistent with regions of high dislocation density promoting deuteride formation, thereby reducing the hysteresis.

3.5. Metallographic analysis

Large pieces of scrap material were available from the fabrication process of all deformed samples. This scrap material was identical to the measured samples except for the *in situ* cooling that was part of the SANS investigation. Specimens were prepared from the Nb8(hc/d) scrap material for TEM analysis and low-temperature electropolishing.

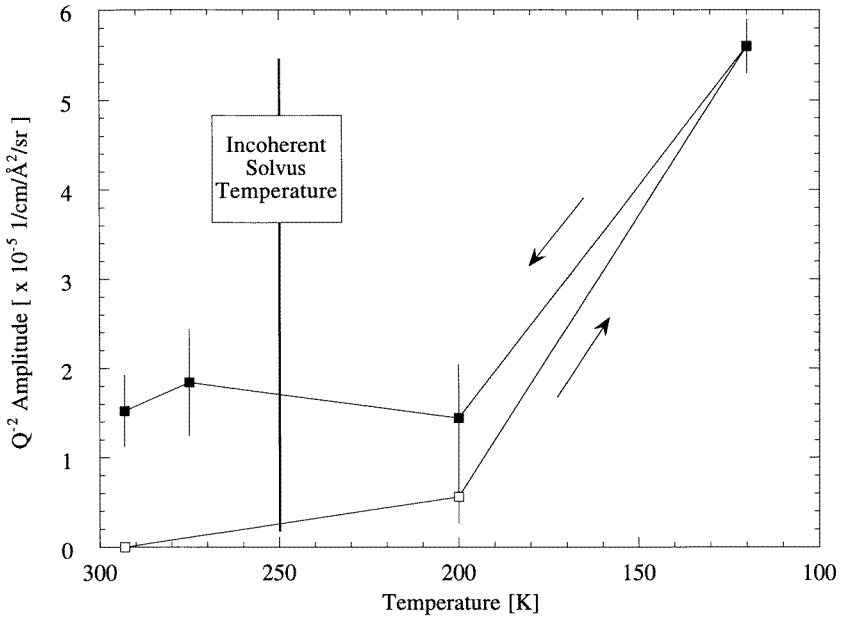

Figure 9. Q^{-2} amplitude for Nb8(hc/d) as a function of sample temperature during *in situ* step-wise cooling and heating. Arrows indicate direction of temperature change.

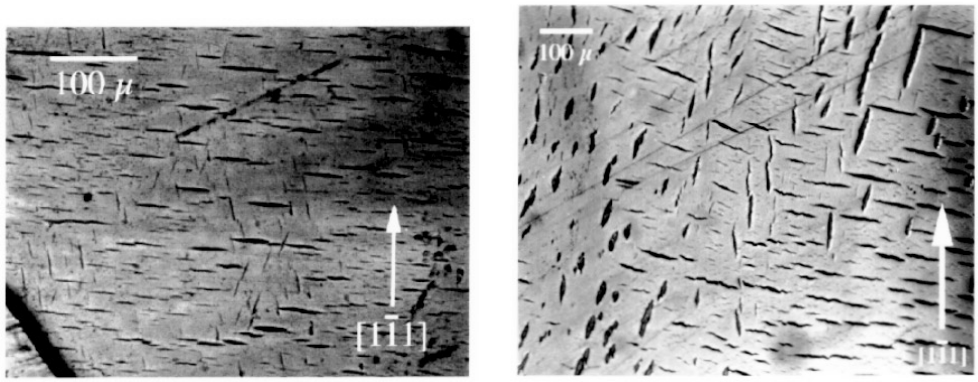

(a) (b)

Figure 10. (a) Micrograph of Nb8(hc/d) scrap material electropolished at 215 K. The plane of the micrograph corresponds to the (110) Q plane of the SANS measurements. The [1$\bar{1}$1] rolling direction is oriented vertically. (b) Micrograph of Nb8(hc/d) scrap material electropolished at 215 K. The plane of the micrograph is ($\bar{1}$12). This plane is perpendicular to the (110) sample face. The [1$\bar{1}$1] rolling direction is again oriented vertically.

Figures 10(a) and 10(b) are room temperature surface micrographs of a Nb8(hc/d) specimen after electropolishing at 215 K. This temperature is well below the β-phase solvus line at 24500 appm (approximately 250 K) and just below the $\alpha + \beta \rightarrow \alpha + \varepsilon$ triple line (225 K) [10]. Temperature reduction associated with electropolishing was the only time the specimens were cooled into the two phase region. The same is true for the TEM specimens.

The line-like structures shown in figure 10(a) are the remnants of the deuteride particles (large plates which have intersected the free surface) caused by preferential etching during the low temperature electropolishing procedure. The plane of this micrograph is the measured (110) Q plane with the $[1\bar{1}1]$ rolling direction vertical. Although line remnants with other orientations are evident in figure 10(a), the vast majority are perpendicular to the rolling direction. This is not proof that the majority of *plates* are perpendicular to the rolling direction since the intersection of the plates with only a single free surface is imaged in the micrograph.

The surface shown in figure 10(b) is a plane perpendicular to the (110) Q plane of figure 10(a) and contains the $[1\bar{1}1]$ rolling direction, again oriented vertically. (In other words, the plane normal of figure 10(b) is given by the cross product of $[1\bar{1}1]$ and [110].) The orientation of figures 10(a) and 10(b) relative to the sample geometry during neutron exposure is shown in figure 11. Two different intersection orientations are seen in figure 10(b), demonstrating that a unique orientation of deuteride plates does not exist.

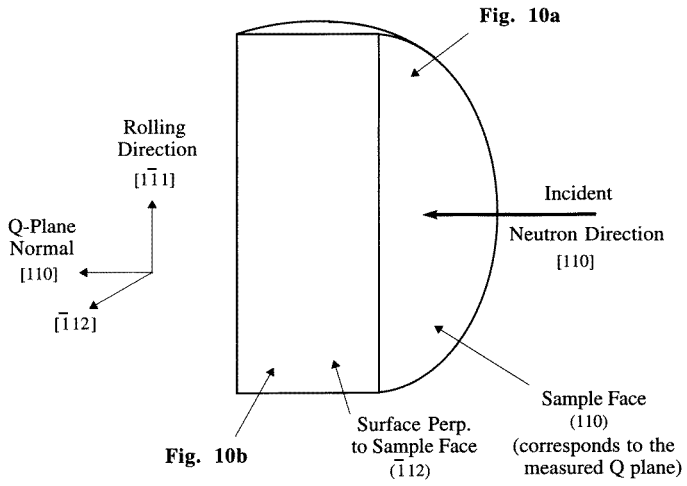

Figure 11. Schematic representation of sample orientation during SANS investigation. Incident neutron beam direction, rolling direction, and orientation of the micrographs in figures 10(a) and (b) are given.

Two conditions on the orientation of the deuteride plates must be met to explain the observed anisotropic SANS response from the deformed samples. First, a significant fraction of all deuteride plates must have normal directions within $\pm 15^\circ$ of the measured Q plane. This is the approximate angular FWHM of the anisotropic behaviour quantified in figures 5 and 6, but applied orthogonally to the Q plane. All plates that satisfy this condition will necessarily have intersection remnants perpendicular to the rolling direction (horizontal in figure 10(b)). By the same argument, deuteride particles with non-horizontal intersection orientations in figure 10(b) cannot contribute to the SANS response that has been observed in these measurements. Second, a necessary requirement for the strong *anisotropy* scattering observed from the deformed samples is that a majority of all plates meeting the first condition have normal directions along the $[1\bar{1}1]$ rolling direction. These plates, and only these plates, will result in horizontal intersection remnants in both figures 10(a) and 10(b). If this were not true, if a more random orientation of plates with normal directions in the measured Q plane existed, the observed Q^{-4} response would have been more isotropic. In the absence of

proof to the contrary, it is now logical to attribute (i) the strong Q^{-4} anisotropy observed within the (110) Q plane and (ii) the preferential arrangement of a majority of the line-like remnants in figure 10(a) to planes which must be aligned orthogonal to the rolling direction.

Hydride particles similar to the plate-like morphology found here have been observed by Birnbaum *et al* in a well-annealed Nb-1.15 at.% hydrogen alloy cooled slowly, under equilibrium conditions, into the two phase region [19]. Hydride plates were observed to form on the $\{100\}_\alpha$ family, as expected from the work of others [9]. Under more rapid cooling conditions ($\sim$2 K min^{-1}), a spherical or 'blocky' hydride morphology was observed by Birnbaum *et al* [19]. We believe a similar effect is responsible for the morphology observed here; the plate-like structures are the result of the dislocation substructure facilitating heterogeneous precipitation, leading to the deuteride particle shape similar to that observed by Birnbaum *et al* under equilibrium cooling conditions in the undeformed Nb matrix.

3.6. TEM analysis

The purpose of room temperature TEM investigation was to characterize the dislocation substructure in the heavily deformed single crystal Nb matrix. Low-temperature TEM analysis was not performed.

Two TEM micrographs of Nb8(hc/d) are shown in figures 12(a) and 12(b). These specimens were made from a piece of Nb8(hc/d) scrap material. The zone axis for these micrographs are the $[1\bar{1}1]$ rolling direction (figure 12(a)) and the $[\bar{1}13]$ direction (figure 12(b)). The latter is approximately 10° off the $[\bar{1}12]$ plane-normal direction of figure 10(b). The substructure shown in figures 12(a) and 12(b) is typical of a cellular dislocation arrangement; the linear features are dislocation bands or cell walls that formed

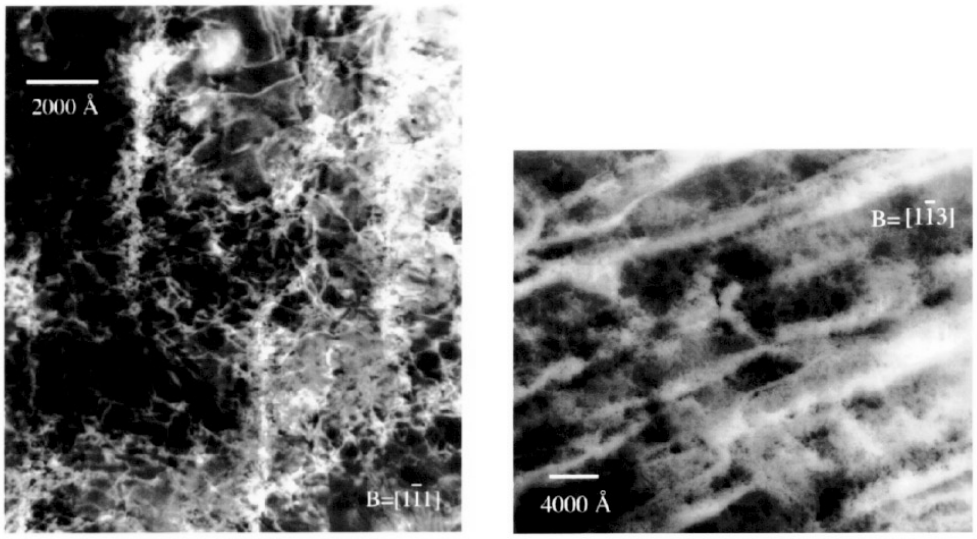

(a) (b)

Figure 12. (a) TEM micrograph of Nb8(hc/d) specimen (made from scrap material). Zone axis of the micrograph is the $[1\bar{1}1]$ rolling direction. The light bands are dislocation cell walls comprised on many dislocations bunched together. (b) TEM micrograph of Nb8(hc/d) specimen (made from scrap material). Zone axis of the micrograph is $[\bar{1}13]$. The light bands are dislocation cell walls comprised on many dislocations bunched together.

during rolling and separate regions of low dislocation density. Similar structures have been observed in deformed, single crystal Nb [20, 21].

A cellular dislocation substructure is often observed in metals driven into the work hardening regime. The ideal use of TEM analysis would be to establish a correlation between the orientation of the large plates shown in figure 10(a) and the dislocation cell structure. This would require, at the very least, analysis of the [110] zone axis corresponding to the measured Q plane and the plane of figure 10(a). This was not possible for the present work.

4. Conclusions

Low temperature deuteride precipitation in well annealed and cold worked single crystal Nb has been characterized in a series of *in situ* SANS measurements. Samples were prepared with low (∼7000 appm) and high (∼24 500 appm) concentrations of deuterium. All samples were in solid solution at room temperature. Two of the samples were deformed by rolling at room temperature to 50% thickness reduction. The following conclusions are drawn from analysis of the SANS measurements:

(i) The observed low temperature SANS response from the undeformed samples was consistent with the formation of spherical deuteride particles. For two samples with approximately the same deuterium concentration (∼7200 appm), the cooling rate (continuous cooling at a rate of 2–3 °C min^{-1} versus step-wise cooling) had a noticeable effect on the Porod scattering amplitude; continuous cooling resulted in an 8.1 increase in scattering intensity. This observation is consistent with the more rapid, direct cooling rate inducing precipitation on a much finer scale. For the stepwise cooling procedure applied to two samples with different deuterium concentrations, the low-Q Porod scattering amplitude varied in proportion to the concentration. This is consistent with the formation of deuteride particles in numbers proportional to the overall concentration under more equilibrium cooling conditions.

(ii) The effect of deformation by rolling on the observed low temperature SANS response was significant. The scattering pattern exhibited marked two-fold asymmetry in the Porod region (where the Q^{-4} scattering dominates the measured response), with the direction of maximum scattering along the $[1\bar{1}1]$ rolling direction. This is attributed to the formation of large, oriented deuteride particles with a plate-like morphology. In addition, the development of an isotropic Q^{-2} response at high Q was observed in the deformed samples. This is the single particle form factor for plate-like particles and is attributed to the formation of much smaller deuteride plates with a more random orientation distribution. The volume fraction of these smaller platelets was approximately 10% of the total precipitated deuteride phase.

(iii) The SANS response as a function of temperature was recorded for two samples. A noticeable hysteresis was evident in the undeformed sample temperature response. Such hystereses are generally thought to be due to irreversible formation of dislocations at the incoherent deuteride boundary. The temperature dependence of the low-Q Porod response and the Q^{-2} response for the deformed sample were analysed separately. Both responses tracked closely together during temperature change, indicating the hysteresis was greatly reduced by deformation. This is expected if preferential nucleation of the deuteride phase at regions of high dislocation density occurs. The onset of the Q^{-2} scattering behaviour in the deformed sample was shifted to temperatures well below the solvus observed for the Porod scattering, consistent with a smaller amount of deuterium available for deuteride precipitation into the smaller platelets.

In addition to SANS, metallographic and TEM analysis were performed on the deformed, high concentration sample. The following conclusions are derived from this analysis:

(iv) Metallographic analysis of low temperature electropolished scrap material taken from the deformed, high concentration sample was performed to characterize the orientation of the large plate-like deuteride particles. Analysis of two polished surfaces showed the presence of large line-like remnants that resulted from preferential etching of the deuteride particles. The majority of these remnants on the surface coinciding with the measured Q plane had orientations consistent with the anisotropic SANS response observed in the Porod regime. The platelets responsible for the Q^{-2} scattering behaviour are thought to be too small to observed with an optical microscope.

(v) TEM analysis of specimens taken from the deformed, high concentration scrap material was also performed. A distinct cellular dislocation substructure was observed in the deformed Nb matrix. It was not possible for the present work to establish a correlation between the orientation of the dislocation cell walls the line-like remnants observed in the electropolished samples.

These conclusions taken together indicate that deformation of single crystal Nb affects the deuteride phase transformation in a fundamental way. We believe the large plate-like particle morphology is the result of an interaction with the cellular dislocation substructure. One possible explanation is that the deuterium-dislocation interaction, which initially traps deuterium at individual dislocations, results in the cell walls acting as a nucleation framework. Alternatively, an elastic stress field interaction acting over longer length scales (compared with the more short-range interaction with individual dislocations) induces the highly anisometric deuteride particle shape. This second explanation is somewhat analogous to the formation, under equilibrium conditions, of the hydride phase in plates perpendicular to the elastically soft [100] directions in the host Nb matrix. However, in the present case precipitation of the plate-like deuteride particles is not controlled by the elastic properties of the Nb fcc lattice, but by the elastic state within the dislocation cell structure.

The effect of deformation on the temperature hysteresis is consistent with the above remarks. Preferential low-temperature hydride nucleation at regions of high dislocation density has been observed in Nb with TEM [6]. The large degree of local lattice distortion at these sites reduces or eliminates the need for additional dislocation generation at the incoherent boundary. Thus, the same elastic interactions that alter the particle morphology are also expected to reduce the observed temperature hysteresis, as was observed.

Acknowledgments

The authors acknowledge the support of the National Science Foundation under Grant No DMR-9496297. The SANS measurements were performed at Intense Pulsed Neutron Source at Argonne National Laboratory. This facility is supported by the US DOE, BES-Materials Sciences, under contract No W-31-109-ENG-38. TEM analysis was carried out in the Center for Microanalysis of Materials at the University of Illinois, which is supported by the US DOE under grant DEFG02-91-ER45439.

We also appreciate the assistance given to us by Mr B Kestel (MSD-ANL), Mr D Wozniak (IPNS-ANL) and Dr P Thiyagarajan (IPNS-ANL). Finally, the authors are grateful to Dr J King (University of Michigan) for overall interest in the project, to Dr J Stubbins (University of Illinois) for help with selected area diffraction patterns, and to Dr H Birnbaum (University of Illinois) for useful comments.

References

[1] Horner H and Wagner H 1974 *J. Phys. C: Solid State Phys.* **7** 3305–25
[2] Wagner H 1978 *Topics in Applied Physics, Hydrogen in Metals I* ed G Alefeld and J Völkl (Berlin: Springer) p 5–51
[3] Zabel H and Peisl J 1979 *J. Phys. F: Met. Phys.* **9** 1461–76
[4] Zabel H and Peisl H 1979 *Phys. Rev. Lett.* **42** 511–14
[5] Wagner H and Horner H 1974 *Adv. Phys.* **23** 287
[6] Schober T 1975 *Phys. Status Solidi* A **30** 107–16
[7] Schober T 1975 *Phys. Status Solidi* A **29** 395–406
[8] Makenas B J and Birnbaum H K 1982 *Acta. Metall.* **30** 469–81
[9] Schober T and Wenzl H 1978 *Topics in Applied Physics, Hydrogen in Metals II* ed G Alefeld and J Völkl (Berlin: Springer) p 11–71
[10] Smith J F 1983 *Bull. Alloy Phase Diagr.* **4** 39–46
[11] Maeland A J, Libowitz G G, Lynch J F and Rak G 1984 *J. Less-Common Metals* **104** 133–9
[12] Thiyagarajan P, Epperson J E, Crawford R K, Carpenter J M, Klippert T E and Wozniak D G 1997 *J. Appl. Cryst.* **30** 280–93
[13] Roth M 1977 *J. Appl. Cryst.* **10** 172–6
[14] Feigin L A and Svergun D I 1987 *Structure Analysis by Small-Angle X-Ray and Neutron Scattering* ed G W Taylor (New York: Plenum)
[15] Porod G 1982 *Small Angle X-ray Scattering* ed O Glatter and O Kratky (London: Academic) p 17–51
[16] Heuser B J, King J S, Summerfield G C, Boue F and Epperson J E 1991 *Acta Metall. Mater.* **39** 2815–24
[17] Heuser B J and King J S *J. Alloys Compounds* at press
[18] Westlake D G and Ockers S T 1975 *Metallurg. Trans.* A **6** 399–402
[19] Birnbaum H K, Grossbeck M L and Amano M 1976 *J. Less-Common Metals* **49** 357–70
[20] Taylor G and Christian J W 1967 *Phil. Mag.* **15** 893–929
[21] Stiegler J O, Dubose C K H, Reed R E Sr and McHargue C J 1963 *Acta. Metall.* **11** 851–60